Phase transformation of the L1$_2$ phase to kappa-carbide after spinodal decomposition and ordering in an Fe–C–Mn–Al austenitic steel

Wei-Chun Cheng [a,*], Chih-Yao Cheng [a], Chia-Wei Hsu [a], David E. Laughlin [b]

[a] Department of Mechanical Engineering, National Taiwan University of Science and Technology, 43 Keelung Road, Section 4, Taipei 106, Taiwan
[b] Department of Materials Science and Engineering, Carnegie Mellon University, 5000 Forbes Avenue, Pittsburgh, PA, USA

ARTICLE INFO

ABSTRACT

Fe–C–Mn–Al steels have the potential to substitute for commercial Ni–Cr stainless steels. For the development of Fe–C–Mn–Al stainless steels, phase transformations play an important role. Our methods of studying the phase transformations of the steel include heating, cooling, and/or annealing. The results of our study show that spinodal decomposition, an atomic ordering reaction and the transformation of the L1$_2$ phase to kappa-carbide occur in the Fe–C–Mn–Al steel. After cooling, the austenite decomposes by the spinodal mechanism into solute-lean and solute-rich austenite phases. The solute-rich austenite phase also transforms into the L1$_2$ phase via the ordering reaction upon cooling to lower temperatures. After quenching and prolonged annealing, the L1$_2$ phase grows in the austenite and finally transforms into kappa-carbide. This L1$_2$ phase to kappa-carbide transformation has not been observed previously.

© 2015 Elsevier B.V. All rights reserved.

1. Introduction

Fe–C–Mn–Al steels which are inexpensive and less dense than the steels have the potential to replace the commercial Ni–Cr stainless steels. In order to commercialize the Fe–C–Mn–Al stainless steels, the basic properties such as mechanical properties and constituent phases of the steels after the phase transformations must be clarified. The phases of the Fe–C–Mn–Al steels at the iron rich side include face-centered cubic (FCC) austenite, body-centered cubic (BCC) ferrite, cementite and simple cubic (SC) kappa-carbide (κ-carbide, or κ-phase) [1]. These phases may coexist under conditions depending on the compositions, temperatures, and even their heating and/or cooling processes. In the Fe–C–Mn–Al steels, various cooling processes from high temperatures can result in different phase transformations, such as Widmanstätten side-plate formation [2], massive transformation [3,4], martensitic transformation [5–7], and spinodal decomposition [8–15].

Spinodal decomposition may occur in a multi-component phase which separates into two other low temperature phases upon cooling [16,17]. A requirement for the occurrence of the spinodal reaction is that the parent and product phases must have the same crystal structure. Spinodal decomposition takes place uniformly throughout the material producing a modulated structure, and is characterized on a phase diagram with a miscibility gap. Phase separation occurs spontaneously when the material is cooled into the unstable region of the miscibility gap, the so-called spinodal regime, which has no chemical energy barrier to the reaction. Spinodal decomposition has been found in various alloy systems, such as Cu–Ti [18,19], Ni–Ti [20,21], Fe–C–Al [22,23], and Fe–C–Mn–Al alloys [8–15]. The occurrence of the spinodal decomposition in the Fe–C–Mn–Al steels results in the decomposition of high temperature FCC austenite into low temperature austenite and L1$_2$ phase [8–15]. The L1$_2$ phase with a Cu$_3$Au structure which is a crystallographic derivative structure from the austenite and has the Pm$\bar{3}$m space group [13]. Note that the crystal structure of L1$_2$ phase is SC which is not the same as the FCC austenite. The requirement of the spinodal decomposition is the same crystal structure of parent and product phases. Thus, the L1$_2$ phase is not the direct product from spinodal decomposition, but most likely from an ordering reaction of the solute-enriched low temperature FCC austenite phase. To date, studies of spinodal decomposition in the Fe–C–Mn–Al steels have not pointed out that spinodal decomposition and ordering reaction occur sequentially to produce the resultant characteristic microstructures consisting of a disordered austenite phase and an ordered L1$_2$ phase [18–21].

After the coherent ordered L1$_2$ phase has formed and grown within the prior austenite grain after quenching and annealing, lamellae of austenite, ferrite, and/or κ-carbide may develop in the Fe–C–Mn–Al steels from the discontinuous (cellular) reaction [13,15] similar to that in Cu-based alloys [24–26]. The SC κ-carbide ((Fe,Mn)$_3$AlC$_x$) precipitating at the grain boundaries belongs to inter-granular carbide, and the modulated coherent L1$_2$ phase ((Fe,Mn)$_3$Al) containing more carbon concentration than the austenite is a carbon-enriched phase. Both SC κ-carbide and SC L1$_2$

* Corresponding author.
 E-mail address: weicheng@mail.ntust.edu.tw (W.-C. Cheng).

phase are of similar crystal structure; however, they contain different amounts of carbon atoms. Even though there are studies on the prolonged annealing of the Fe–C–Mn–Al steels, there is little research on the L1$_2$ phase to κ-carbide transformation. κ-Carbide is a brittle phase and may be the major reason for the decay of the mechanical properties of the steels after prolonged annealing [13]. Below, we show that upon annealing, the L1$_2$ phase transforms into κ-carbide during coarsening.

2. Experimental procedures

Slabs with a composition of Fe–17.9 wt% Mn–7.1 wt% Al–0.85 wt% C were prepared by induction melting. Commercial 1020 steel, carbon, electrolytic manganese, and high purity aluminum were melted together and cast into 3-kg ingots. The ingots were homogenized at 1473 K for 4 h under a protective argon atmosphere, hot forged into steel plates, and annealed to assure composition uniformity. The steel plates were cold rolled to thin plates with a thickness of 2 mm, and cut into specimens with dimensions of 15 mm × 10 mm. The steel samples were heated at 1373 K for 1 h in a protective argon atmosphere, and followed by either quenching in water or air cooling to room temperature. The as-quenched specimens were sealed in quartz tubes under vacuum and held isothermally at low temperatures ranging from 1173 K to 873 K for 1 h, 25 h, and/or 100 h.

The samples were sectioned, polished mechanically and etched in a 5% nital solution for observation in an optical microscope and a Jeol JEM 6500F high resolution field-emission scanning electron microscope (SEM). Some samples were also examined by X-ray diffraction (XRD) in a Rigaku DMAX-B X-ray diffractometer operated at a power of 12 kW. Samples used for observation by a transmission electron microscope (TEM) were polished mechanically into thin foils about 80 µm in thickness, punched into disks of a diameter 3 mm, and electropolished using a twin jet polisher in a 90% CH$_3$COOH and 10% HClO$_4$ solution at room temperature. The TEM samples also underwent ion milling to polish the thin areas in an ion miller. The samples were examined in the Jeol JEM 2010 TEM operated at 200 kV. The possible maximum tilt angles of the TEM specimens are $\pm 45°$ and $\pm 34°$ in the x- and y-axes, respectively.

3. Results and discussion

Fig. 1 shows the results of the investigation of the Fe–C–Mn–Al steel after solution heat treatment at 1373 K and quenching to room temperature water. An optical micrograph (OM) in Fig. 1
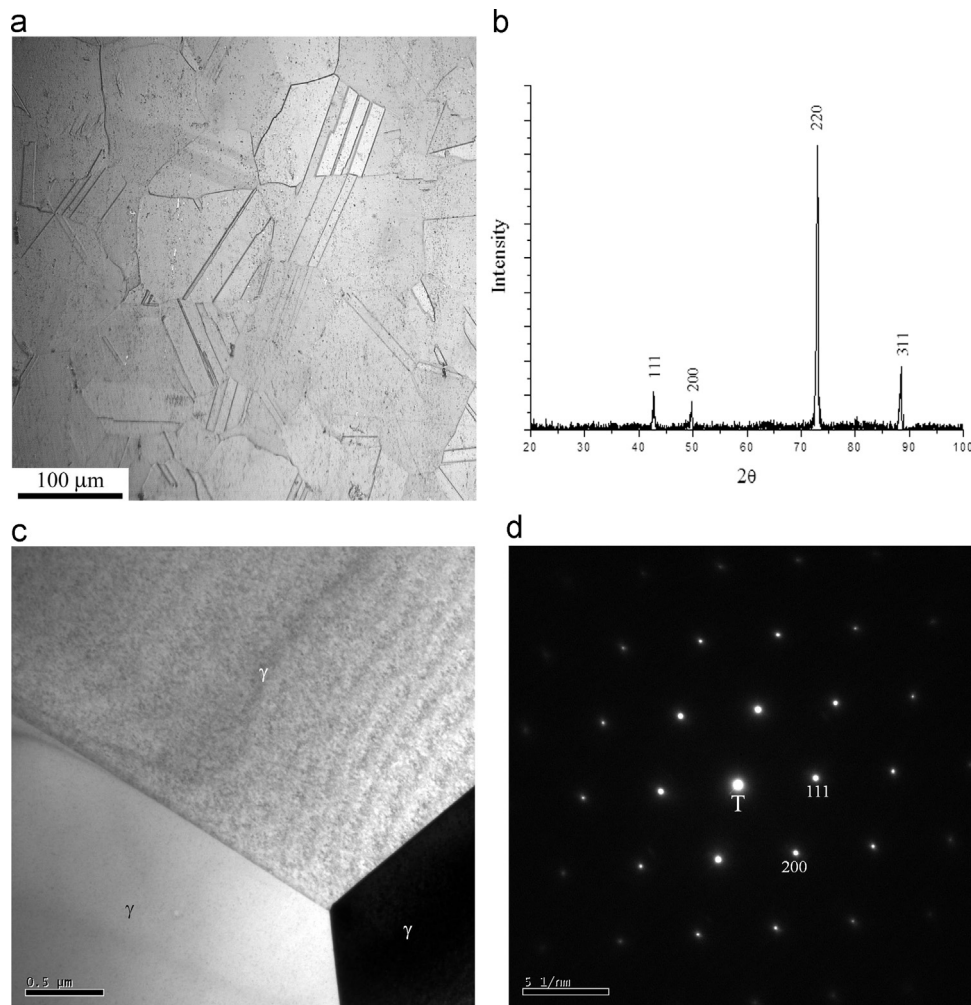
Fig. 1. The analyses of the Fe–C–Mn–Al steel after heating at and quenching from 1373 K: (a) the OM showing that the steel is composed of single phase grains with twins, (b) the XRD displaying that only FCC austenite peaks appear in the steel, (c) the BF image revealing three austenite grains (γ) meeting together, and (d) the SAD pattern from the [01$\bar{1}$] austenite (T: transmission electron beam).

(a) reveals that the steel is composed of about 100-μm grains with twins. An XRD analysis in Fig. 1(b) illustrates that only FCC austenite peaks appear in the steel. The TEM bright-field (BF) image in Fig. 1(c) displays a portion of three austenite grains (γ) of the steel. The accompanying selected area diffraction (SAD) pattern in Fig. 1 (d) is taken from the austenite with the zone axis along the [01$\bar{1}$] direction. Therefore, the high-temperature phase of the Fe–C–Mn–Al steel at 1373 K is confirmed as the austenite.

We have also studied the constituent phases of the steel after heating to 1373 K and air cooling to room temperature, and have found by TEM that $L1_2$ phase appears in the austenite. The results of the TEM investigation are shown in Fig. 2. $L1_2$ superlattice reflections can be seen in the SAD pattern, as shown in Fig. 2(a), which are with the zone axes along the $L1_2$ [001] and austenite [001] directions. These superlattice reflections are barely visible. Some Miller indexes of the austenite reflections are underlined to distinguish them from those of $L1_2$ reflections. In Fig. 2(b), the dark-field (DF) image from the $L1_2$ (100) superlattice reflection shows the uniform distribution of the fine coherent $L1_2$ particles in the austenite. The accompanying BF image in Fig. 2(c) displays that the austenite matrix is not smooth and has periodic strain fields associated with it. Therefore, after air cooling of the Fe–C–Mn–Al steel from 1373 K, the high temperature austenite has already transformed into low temperature austenite and $L1_2$ phases.

Samples display no precipitates in the austenite after heating at 1373 K, cooling (either quenching or air cooling), isothermal holding at 1148 K and/or above temperatures, and quenching to room temperature. Therefore, the steel consists of single phase austenite at temperatures ranging from 1373 K to 1148 K. Upon annealing the quenched steel samples at temperature below 1148 K, we have found that κ-carbide precipitates at the austenite grain boundaries. Below 1098 K, besides the κ-carbide, grain boundary ferrite also appears. Furthermore, lamellae of austenite, ferrite and/or κ-carbide develop from the grain boundaries at temperatures below 1023 K via the discontinuous reaction similar to that in Cu-based alloys [24–26]. The occurrence of the discontinuous reaction is illustrated in the TEM micrographs as shown in Fig. 3 for the Fe–C–Mn–Al steel after 973-K isothermal holding. The BF image in Fig. 3(a) illustrates that the grain boundary precipitates appear in the form of a small colony which is composed of lamellar austenite, ferrite (α) and κ-carbide (κ). Twins also appear in the lamellar austenite grains. The corresponding SAD patterns from the lamellar grains are shown in Fig. 3 (b)–(d). The SAD pattern in Fig. 3(b) is taken from [01$\bar{1}$] austenite, that in (c) is from [$\bar{1}$11] ferrite, and in (d) is from the [$\bar{1}$14] κ-carbide. The lamellae of austenite, ferrite, and κ-carbide nucleate at the grain boundary and grow into the austenite matrix. Similar findings have been reported elsewhere [28]. Therefore ferrite and
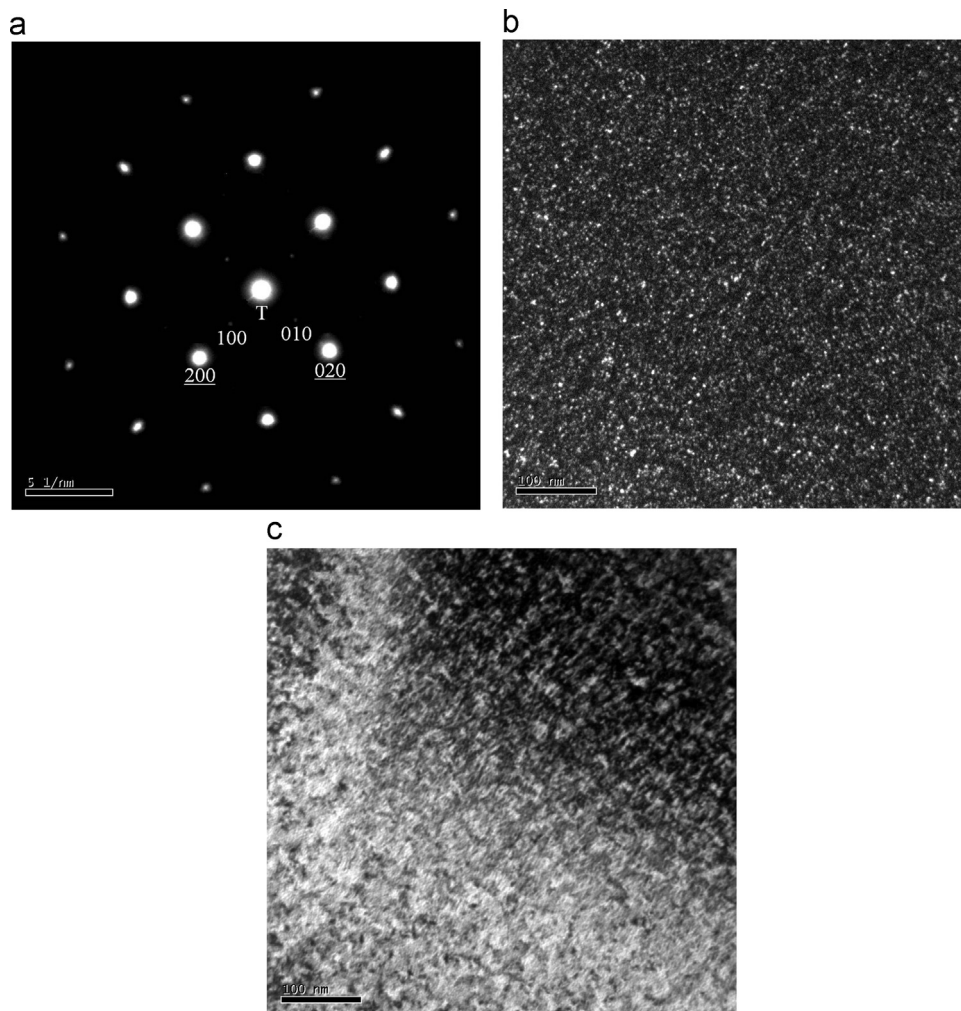
Fig. 2. TEM micrographs of the austenite matrix of the steel after air cooling from 1373 K: (a) the SAD pattern from [001] $L1_2$ phase and [001] austenite, (b) the DF image from the $L1_2$ (100) superlattice reflection showing the fine $L1_2$ particles, and (c) the accompanying BF image.
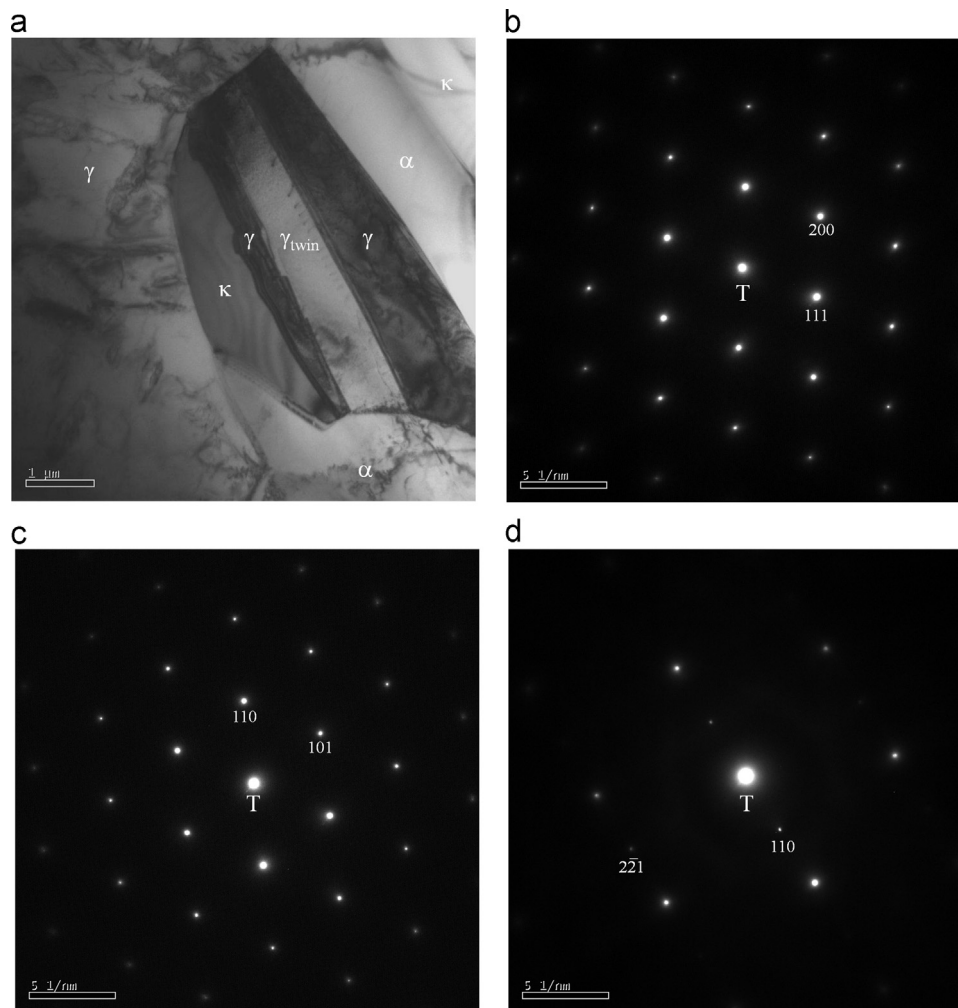
Fig. 3. The TEM analyses of the steel after quenching and holding isothermally at 973 K for 100 h: (a) the BF image showing lamellae of (austenite (γ)+ferrite (α)+κ-carbide (κ)) in the austenite; (b)–(d) the SAD patterns: from (b) [01$\bar{1}$] austenite, (c) [$\bar{1}$11] ferrite, and (d) [$\bar{1}$14] κ-carbide.

κ-carbide are stable low temperature phases in the Fe–C–Mn–Al steel.

The L1$_2$ phase appears in the austenite not only after air cooling from 1373 K, but also after quenching and annealing at temperatures below 1023 K. For example, upon annealing the steel at 873 K for 100 h, fine L1$_2$ particles precipitate in the austenite as shown in the TEM micrographs of Fig. 4. In Fig. 4(a), the DF image from the (100) superlattice reflection reveals that fine modulated L1$_2$ particles form homogeneously in the austenite matrix. The accompanying BF micrograph in Fig. 4(b) shows the non-smooth austenite matrix with periodic strain fields. In Fig. 4(c), the corresponding SAD pattern is from the [0$\bar{1}$1] L1$_2$ phase and [0$\bar{1}$1] austenite. Similar modulated L1$_2$ particles presenting in the austenite have been found in other Fe–C–Mn–Al austenitic steels [8–15]. Spinodal decomposition has been attributed to occurring in the Fe–C–Mn–Al austenitic steels after quenching and annealing [8–15].

A series of annealing processes have been carried out to measure the upper temperature limit for the existence of the L1$_2$ phase. The TEM micrographs in Fig. 5 show the appearance of the L1$_2$ phase near the upper temperature limit of the L1$_2$ phase. The DF image in Fig. 5(a) and the accompanying BF image in Fig. 5 (b) display the L1$_2$ particles in the austenite after quenching from 1373 K and annealing at 998 K for 1 h. Small non-uniform cuboid

L1$_2$ precipitates are distributed in the austenite. Another DF and BF micrographs are shown in Fig. 5(c) and (d), respectively, for the steel after 100-h annealing at 998 K. The TEM micrographs show the large precipitates form in the austenite. The rafted structure of the large precipitates is quite similar to that of Ni$_3$Al phase of the Ni-based superalloys [29]. Thus, after prolonged annealing at 998 K, the L1$_2$ phase has grown into large rafted precipitates. However, no L1$_2$ phase has been found in the austenite after annealing at temperatures of 1023 K and/or above. Therefore, the upper temperature limit for the appearance of the L1$_2$ phase is between 1023 K and 998 K.

After heating at and air cooling from 1373 K, the appearance of L1$_2$ phase in the Fe–C–Mn–Al steel is attributed to the occurrence of not only the spinodal decomposition, but also the following ordering reaction. Before the discussion of the spinodal decomposition, we have to bear in mind that one basic criterion for the occurrence of the spinodal decomposition of the alloys is that the parent and product phases are with the same crystal structure [16,17]. When the Fe–C–Mn–Al austenitic steel undergoes the spinodal decomposition, the high temperature FCC austenite must decompose into two other low temperature FCC austenite phases, rather than directly into low temperature FCC austenite phase and the SC L1$_2$ phase. The L1$_2$ phase is a derivative phase from the austenite, and the crystal structure of SC L1$_2$ phase is not the same
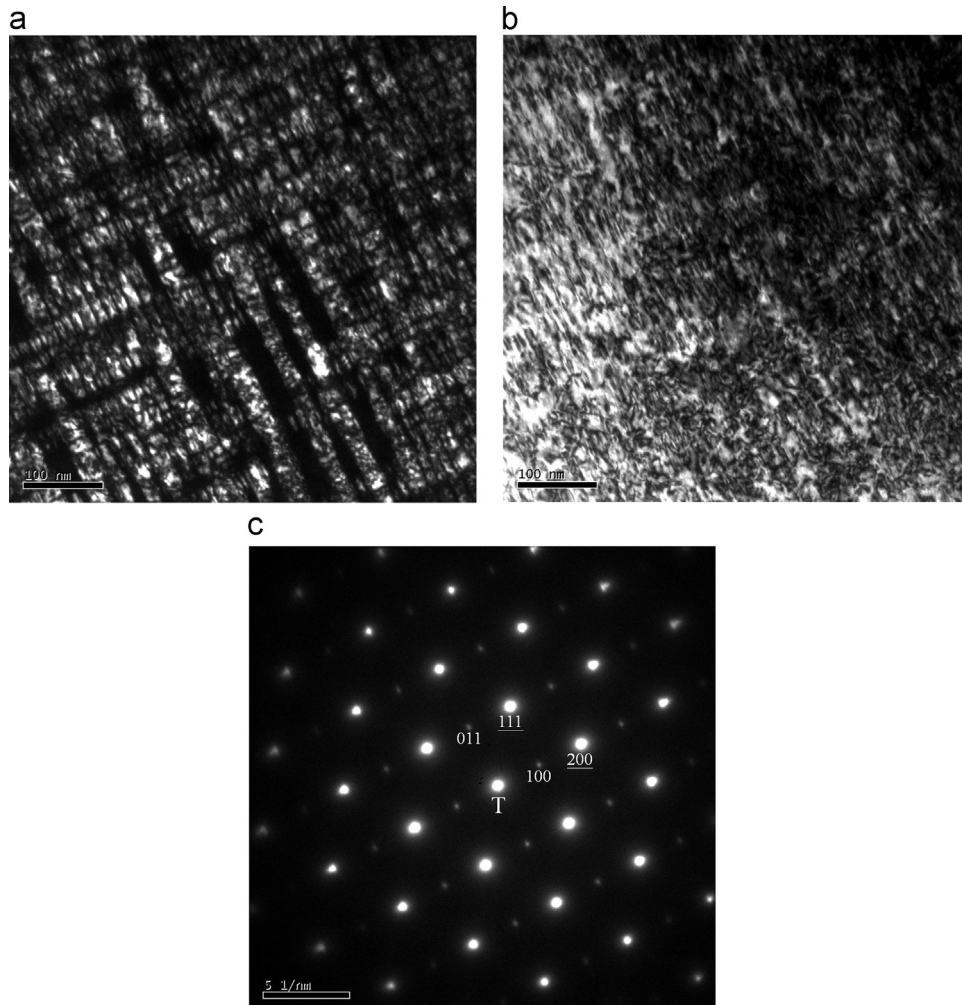
Fig. 4. The TEM investigation of the austenite matrix of the steel after the 100-h isothermal holding at 873 K: (a) the DF image from (100) superlattice reflection showing the uniform distribution of the fine modulated $L1_2$ precipitates, (b) the accompanying BF image, and (c) the SAD pattern from the [$0\bar{1}1$] $L1_2$ phase and [$0\bar{1}1$] austenite. The Miller indexes of the austenite are underlined.

as the FCC austenite. Thus, the $L1_2$ phase is not the direct product phase from the spinodal decomposition, but most likely from another ordering reaction which allows one of the low temperature austenite phases to transform into $L1_2$ phase upon cooling to lower temperature. Therefore, the most possible sequence of the phase transformations of the Fe–C–Mn–Al austenitic steel during cooling is as follows. The spinodal decomposition occurs first and results in the decomposition of the high temperature austenite (γ) into two other FCC austenite phases with which one austenite phase (γ') is solute-lean and the other (γ'') is solute-rich. Upon cooling to lower temperature, the solute-rich austenite transforms into the $L1_2$ phase following the ordering reaction. Therefore, the overall phase transformations in the Fe–C–Mn–Al austenitic steel upon air cooling are as follows: $\gamma \rightarrow \gamma' + \gamma''$ and $\gamma'' \rightarrow L1_2$.

For the steel after heating at and quenching from 1373 K, no direct evidence has been found for the appearance of the $L1_2$ phase in the austenite. However, our suggestion is that after quenching, the high temperature austenite should have decomposed into two low temperature austenite phases, one with low solute contents and the other containing rich solute contents, via the spinodal decomposition, and at low temperature the solute-rich austenite should have already transformed into $L1_2$ phase through the ordering reaction. Since the lattice constants of these two low-temperature austenite phases and the $L1_2$ phase are

almost the same, it is difficult to distinguish them from the SAD patterns of the two austenite phases, for example, as shown in Fig. 1(d). As the ordering reaction occurs, the $L1_2$ nuclei form in the austenite at very low temperature. However, the fast cooling during quenching, especially at low temperatures, does not provide much time for the diffusion of solute atoms and the growth of the $L1_2$ nuclei. The small $L1_2$ nuclei are frozen as very fine particles with relative low solute contents in the austenite matrix after the ordering reaction and cannot be detected by TEM. For example, very weak (001) reflections are not shown in the SAD pattern of Fig. 1(d). However, the $L1_2$ nuclei accumulate the solute atoms and grow very fast upon annealing the quenched steel samples at high temperatures, for example, as the DF micrograph shown in Fig. 4 (a). This suggests that after quenching, very fine $L1_2$ nuclei have already existed in the austenite of the steel, but cannot be detected by TEM. Therefore, compared to the phase transformations in the air-cooled steel, the quenched steel should have also undergone the spinodal decomposition and the following ordering reaction.

The morphology of the $L1_2$ precipitates in the austenite changes as the isothermal holding time increases. Different growth stages of the $L1_2$ phase have been investigated by SEM. Secondary electron images (SEIs) in Fig. 6 illustrate the growing features of the $L1_2$ precipitates in the austenite after isothermal holding at 973 K for different periods. The holding periods in Fig. 6 are as
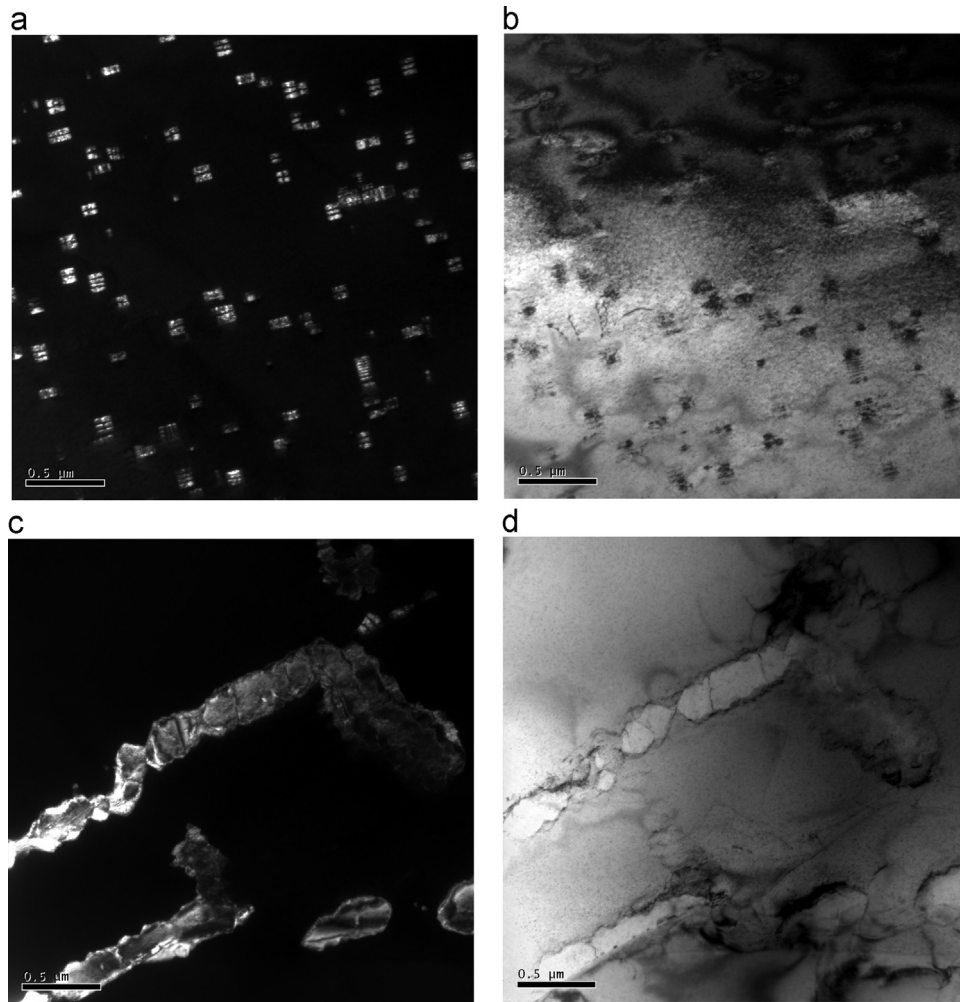
Fig. 5. The TEM micrographs of the steel annealed at 998 K: (a) the DF and (b) accompanying BF images revealing non-uniform distribution of the cuboid $L1_2$ precipitates after 1 h annealing; (c) the DF and (d) corresponding BF micrographs showing large rafted precipitates after annealing for 100 h.

follows: (a) 1 h, (b) 25 h, (c) and (d) 100 h. As the annealing time increases, small modulated particles grow along specific directions into larger rafted precipitates. The SEI in Fig. 6(a) shows κ-carbide also precipitates at the austenite grain boundaries concurrently with the modulated $L1_2$ precipitates in the austenite matrix. In addition, κ-carbide is present with ferrite and austenite in the lamellar colonies which form via the discontinuous reaction as shown in Fig. 6(b) and (c) after 973-K isothermal holding for 25 h and 100 h, respectively. These colonies nucleate at the grain boundaries and grow into the austenite matrix along with the coarsening of the modulated $L1_2$ precipitates in the austenite matrix. The composition trends and the relative heights of the lamellar phases of the Fe–C–Mn–Al have been pointed out in our previous report [27]. κ-Carbide has the highest Mn and Al contents, the ferrite contains the lowest Mn content, and austenite is with the lowest Al content among the lamellar phases. The relative heights of the lamellar phases from highest to lowest in the SEI are as follows: κ-carbide, austenite, and ferrite. We have employed the EDS in SEM to measure the compositions of the constituent phases. Thus, we can identify the lamellar phases without difficulty from the compositions, morphologies, and relative locations of the phases in the lamellae. For example, in Fig. 6(b), we have marked some of the constituent phases in the lamellae. As reported in our previous article [28], after prolonged annealing, the lamellar colonies eventually become the only final products, and thus the

prior austenite with the rafted precipitates disappears.

Fig. 7 shows the results of the TEM investigation on the $L1_2$ precipitates of the steel after isothermal holding at 973 K. The holding time for the steel in Fig. 7(a) and (b) is 1 h, and that in (c) and (d) is 100 h. The $L1_2$ (100) DF image in Fig. 7(a) shows the appearance of modulated $L1_2$ precipitates in the austenite. The corresponding SAD pattern in Fig. 7(b) is from the $[0\bar{1}1]$ $L1_2$ phase and $[0\bar{1}1]$ austenite. Fig. 7(c) and (d) shows another set of the (100) DF image and SAD pattern, respectively, focusing on the large rafted precipitate in the austenite. Note that the SAD pattern in Fig. 7(d) shows no common reflections from both phases; i.e., the reflections from the austenite are no more located at the same reflections from the rafted precipitate. For example, some of the austenite reflections are connected with white lines in Fig. 7(d), and the (011) reflection from the rafted phase is not located at the centered point of the white line two austenite (111) reflections; i.e., it is no more located at the $L1_2$ (011) reflection. To compare the reflections from the rafted precipitate with those from $L1_2$ and κ-carbide, we confirm that the crystal structure of the rafted precipitate belongs to the κ-carbide; i.e., the precipitate in the austenite matrix has been transformed from $L1_2$ into kappa-carbide. The corresponding SAD pattern in Fig. 7(d) shows the separation of the reflections of the κ-carbide from those of the austenite and is from the $[0\bar{1}1]$ κ-carbide and $[0\bar{1}1]$ austenite. Therefore, after quenching from 1373 K and annealing at temperatures below
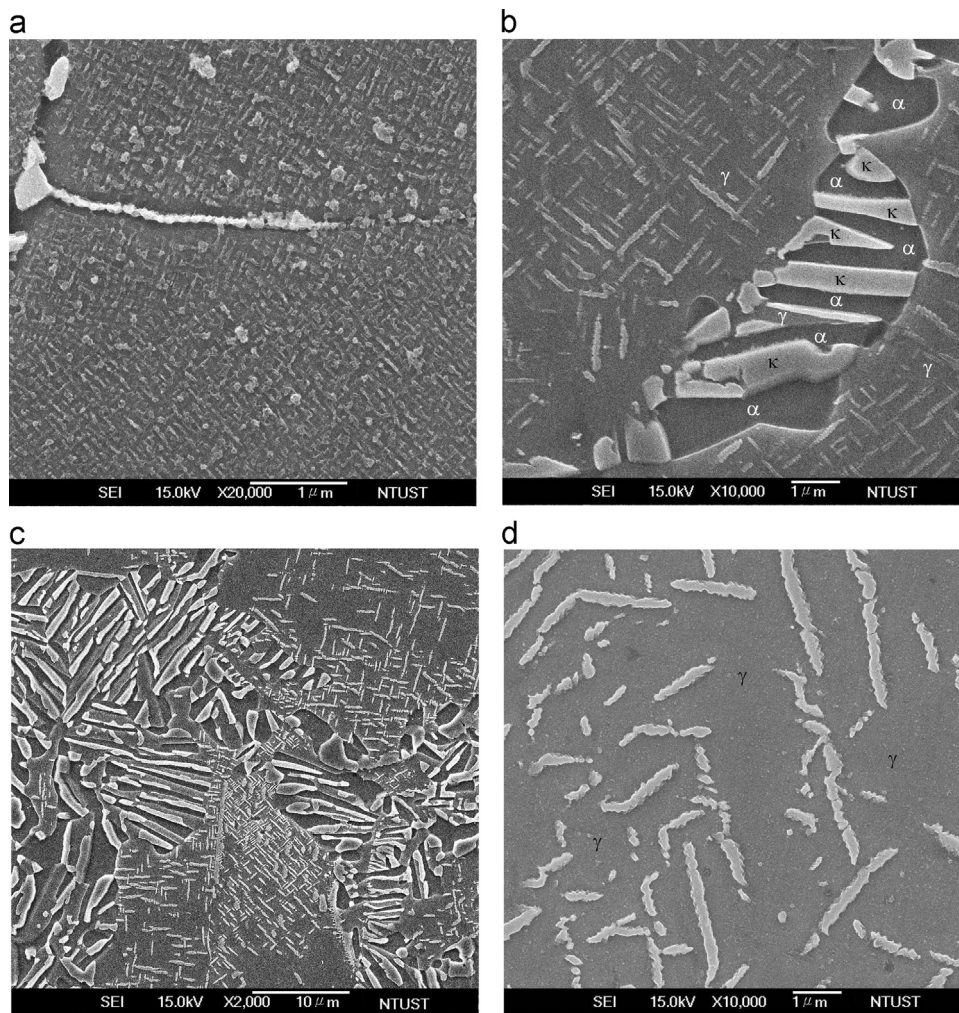
Fig. 6. SEIs showing the different growth stages of the grain boundary precipitates and the modulated precipitates in the austenite matrix after isothermal holding at 973 K for (a) 1 h, (b) 25 h, (c) and (d) 100 h.

998 K, L1$_2$ phase appears initially in the austenite matrix as fine modulated particles, and after prolonged annealing it grows in the form of rafted precipitate and transforms into κ-carbide.

The crystal structures of both SC L1$_2$ phase and SC κ-carbide are similar. However, the L1$_2$ phase is a meta-stable carbon-enriched phase. As the spinodal decomposition and the sequential ordering reaction occur in the Fe–C–Mn–Al steel upon cooling (either quenching or air cooling), the product phases are austenite (γ′) and L1$_2$ phase. The austenite is a carbon-lean phase, while L1$_2$ phase is a carbon-enriched phase. Upon annealing at low temperatures, the L1$_2$ phase grows and consumes the carbon atoms from the neighboring austenite (carbon-lean phase). In addition, the volume fraction of the modulated precipitates decreases when the annealing time increases as shown in Fig. 6. The accumulation of carbon atoms of the modulated precipitates continues upon further annealing, and accompanies with the allocation of the interstitial carbon atoms to the preferential positions of the carbon-enriched phase. When the carbon concentration of the L1$_2$ phase exceeds the critical value for the formation of κ-carbide, L1$_2$ phase transforms into κ-carbide.

4. Conclusions

In the Fe–C–Mn–Al austenitic steel, we have found three significant phase transformations: (1) the spinodal decomposition,

(2) an atomic ordering reaction, and (3) the L1$_2$ phase to κ-carbide transformation. The spinodal decomposition and following ordering reaction occur in the austenitic steel after heating at and cooling (either quenching or air cooling) from 1373 K. The high temperature FCC austenite decomposes into low temperature FCC austenite phases by spinodal decomposition. One austenite phase is solute-lean and the other is solute-rich. The ordering reaction takes place upon further cooling to lower temperature, and the solute-rich FCC austenite transforms into the SC L1$_2$ phase.

Upon annealing the quenched steel at temperatures below 898 K, we have found the appearance of L1$_2$ particles. Very fine L12 nuclei have already existed in the austenite matrix after quenching. The L1$_2$ phase precipitates homogeneously in the austenite as small coherent particles at the initial stage of annealing. However, the L1$_2$ phase accumulates the carbon atoms from the surrounding carbon-lean austenite and grows into large rafted precipitate upon prolonged annealing, and transforms into kappa-carbide. Thus, in the Fe–C–Mn–Al steel, the L1$_2$ phase is a meta-stable phase and the k-carbide is the final stable low temperature phase. Here, we have found that the phase transformations of the austenite after quenching and annealing at temperatures below 998 K include the spinodal decomposition, ordering reaction, and L1$_2$ to κ-carbide transformation as follows: γ→γ′+γ ″→γ′+L1$_2$ and L1$_2$→κ-carbide. The spinodal decomposition and following ordering reaction have never been so clearly identified in the Fe–C–Mn–Al steels. In addition, the L1$_2$ to κ-carbide
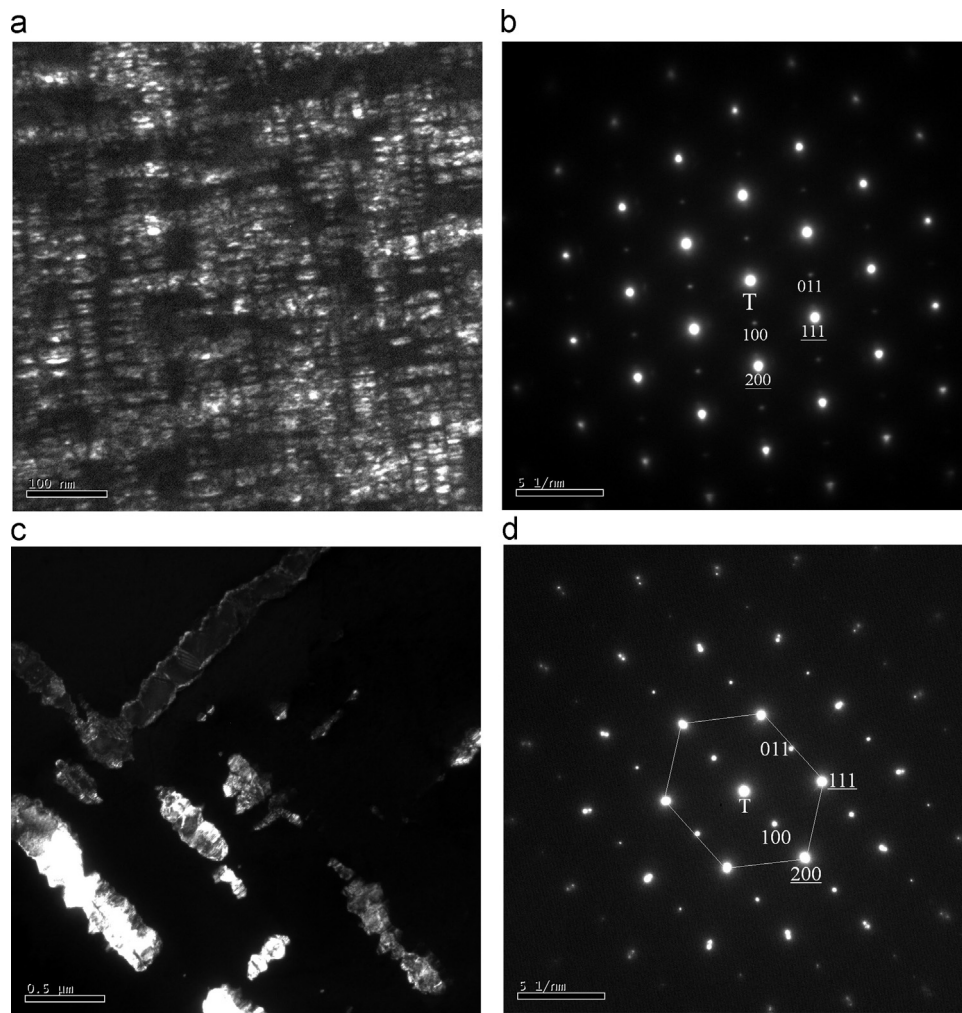
Fig. 7. TEM micrographs of the modulated precipitates in the austenite matrix after annealing at 973 K: (a) the (100) DF image of the L1$_2$ modulated precipitates and (b) accompanying SAD pattern of [0$\bar{1}$1] L1$_2$ and [0$\bar{1}$1] austenite for 1 h isothermal holding; (c) the (100) DF image of the κ-carbide and (d) accompanying SAD pattern of [0$\bar{1}$1] κ-carbide and [0$\bar{1}$1] austenite after 100-h isothermal holding. Note that the L1$_2$ modulated precipitates have transformed into κ-carbide in (c) and (d) after the prolonged annealing.

transformation has never been pointed out before. As the κ-carbide is brittle, it is detrimental to the mechanical property of the Fe–C–Mn–Al steels. Therefore, it is essential to design a new process in the future to avoid the nucleation and growth of the κ-carbide during the steel-making processes.

Acknowledgment

References

[1] K. Ishida, H. Ohtani, N. Satoh, R. Kainuma, T. Nishizawa, ISIJ Int. 30 (1990) 680–686.
[2] W.C. Cheng, Metall. Trans. A 36 (2005) 1737–1743.
[3] W.C. Cheng, H.Y. Lin, C.F. Liu, Mater. Sci. Eng. A 335 (2002) 82–88.
[4] W.C. Cheng, C.K. Lai, Scr. Mater. 55 (2006) 783–786.
[5] W.B. Lee, F.R. Chen, S.K. Chen, G.B. Olson, C.M. Wan, Acta Metall. Mater. 43 (1995) 21–30.
[6] H.Y. Chu, F.R. Chen, T.B. Wu, Scr. Metall. 33 (1995) 1269–1275.
[7] W.C. Cheng, C.F. Liu, Y.F. Lai, Scr. Mater. 48 (2003) 295–300.
[8] K.H. Han, J.C. Yoon, W.K. Choo, Scr. Metall. 20 (1986) 33–36.
[9] K. Sato, K. Tagawa, Y. Inoue, Scr. Metall. 22 (1988) 899–902.
[10] K. Sato, K. Tagawa, Y. Inoue, Mater. Sci. Eng. A 111 (1989) 45–50.
[11] K. Sato, K. Tagawa, Y. Inoue, Metall. Trans. A 21 (1990) 5–11.
[12] K.H. Han, Mater. Sci. Eng. A 197 (1995) 223–229.
[13] W.K. Choo, J.H. Kim, J.C. Yoon, Acta Mater. 45 (1997) 4877–4885.
[14] M.C. Li, H. Chand, P.W. Kao, D. Gan, Mater. Chem. Phys. 59 (1999) 96–99.
[15] C.S. Wang, C.N. Hwang, C.G. Chao, T.F. Liu, Scr. Mater. 57 (2007) 809–812.
[16] J.W. Cahn, Acta Metall. 9 (1961) 795–801.
[17] J.W. Cahn, Acta Metall. 10 (1962) 179–183.
[18] D.E. Laughlin, Acta Metall. 23 (1975) 329–339.
[19] W.A. Soffa, D.E. Laughlin, Prog. Mater. Sci. 49 (2004) 347–366.
[20] W.A. Soffa, D.E. Laughlin, Acta Metall. 37 (1989) 3019–3028.
[21] D.E. Laughlin, Acta Metall. 23 (1975) 329–339.
[22] T. Tadaki, K. Shimizu, T. Watanabe, Trans. J. Inst. Met. 12 (1971) 386–389.
[23] R. Oshima, C.M. Wayman, Metall. Trans. 3 (1972) 2163–2169.
[24] R.C. Ecob, J.V. Bee, B. Ralph, Metall. Trans. A 11 (1980) 1407–1414.
[25] M. Miki, D.E. Laughlin, Metall. Trans. A 16 (1985) 1751–1757.
[26] H.I. Aaronson, C.S. Pande, Acta Mater. 47 (1999) 175–181.
[27] W.C. Cheng, Y.S. Song, Y.S. Lin, K.F. Chen, P.C. Pistorius, Metall. Mater. Trans. A 45 (2014) 1199–1216.
[28] W.C. Cheng, J. Met. 66 (2014) 1809–1820.
[29] F.R.N. Nabarro, Metall. Mater. Trans. A 27 (1996) 513–530.